

Importance of spin-orbit coupling in hybrid organic/inorganic perovskites for photovoltaic applications

Jacky Even,[†] Laurent Pedesseau,[†] Jean-marc Jancu,[†] and Claudine Katan^{‡}*

[†]Université Européenne de Bretagne, INSA, FOTON, UMR 6082, 35708 Rennes, France

[‡]CNRS, Institut des Sciences Chimiques de Rennes, UMR 6226, 35042 Rennes, France

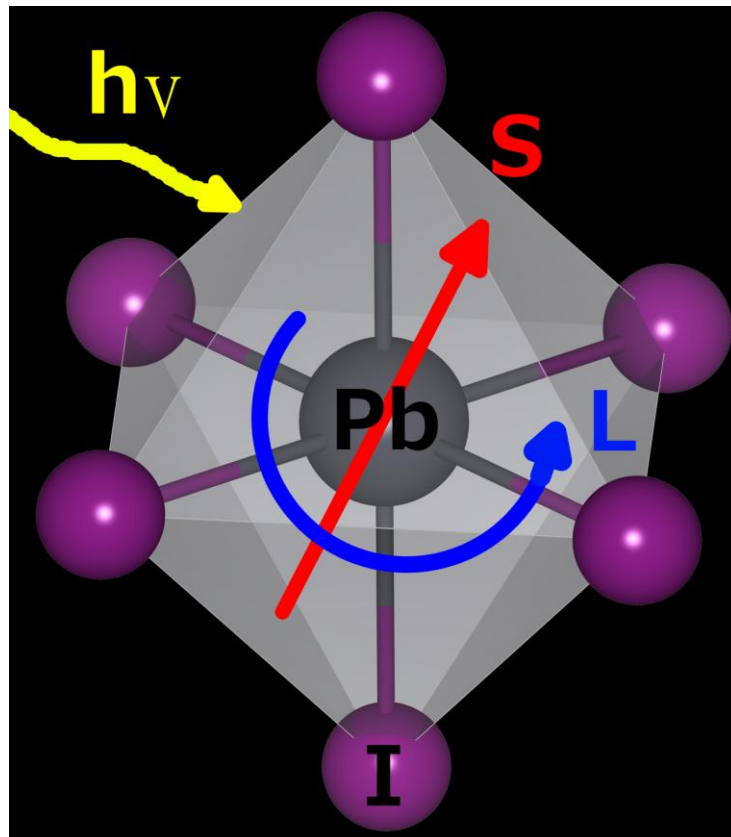
Corresponding Author

Claudine Katan

Three-dimensional organic/inorganic perovskites have recently been suggested as a novel class of materials for dye-sensitized solar cells (DSSC) with improved photo-conversion efficiency. These compounds are modeled in this work within the density functional theory (DFT). The band-gaps are dominated by a giant spin-orbit coupling (SOC) in the conduction-band, which has been largely overlooked so far. Direct and isotropic optical transitions at room temperature are

associated to a spin-orbit split-off band related to a triply degenerated conduction-band of the cubic lattice without SOC. It is shown that, due to the strong SOC, the electronic states involved in the optical absorption are only slightly perturbed by local distortions of the lattice. In addition, band offset calculations confirm that $\text{CH}_3\text{NH}_3\text{PbX}_3/\text{TiO}_2$ ($\text{X}=\text{Br}, \text{I}$) is a reference material for driving electrons toward the electrode in dye-sensitized solar cells. Two dimensional hybrid perovskites are also suggested to reach further flexibility for light conversion efficiency. This study is a major step towards the understanding of the optoelectronic properties of these novel class of DSSC at the level of knowledge already achieved in the field of conventional semiconductors.

TOC GRAPHICS



Hybrid materials, optoelectronics, titanateoxyde, density functional theory

Photovoltaic (PV) solar electricity is one of the key technologies of the 21st century to reduce the world's reliance on fossil fuels for energy generation. Reduced costs and higher conversion efficiencies are of crucial importance to make PV-based technologies economically more competitive. The quest for quality and performances of future solar cells has attracted a vast research effort over the last decade in the field of semiconductor heterostructures, nanostructured materials, and thin films. Various approaches ranging from high-cost/high-performance III-V technologies, multiple junctions and concentrator systems, to low-cost thin-films technologies¹⁻⁴ have been investigated. Obviously, the design of novel and/or efficient PV devices requires a

realistic modeling of underlying material's properties including chemical composition, mechanical, electrical and optical features. This can be gained with state-of-the-art ab-initio approaches. In addition, such knowledge is desirable to reach PV cells composed of earth-abundant elements based materials.

Three-dimensional organic/inorganic perovskites, based on relatively small organic cations, have recently been suggested as a novel class of materials for dye-sensitized solar cells (DSSC) with improved photo-conversion efficiency.⁵⁻¹⁷ Indeed, with a nanoporous TiO₂ electrode, ultra-high light power conversion efficiencies have been demonstrated. Compared to alternative strategies based on inorganic semiconductor quantum dots (QDs) or extremely thin absorbers coated upon the internal surface of a mesoporous TiO₂ electrode, hybrid perovskites offer several benefits. In particular, the ease of synthesis, tailoring of the optical absorption by chemical substitution, electronic transport, and high stability in dry air, are among the most featured properties of these systems. Interestingly, whereas conduction-band and valence-band alignments between absorbers and TiO₂ are of crucial importance in understanding charge transfer and charge transport,^{7,8,16,18} their modeling is still scanty.

Conversely, two dimensional hybrid organic/inorganic materials have attracted increasing interest over the past decade due to their potential optoelectronic applications.¹⁹ Once more, the versatility of the organic part affords the possibility of fine tuning material's properties. For example, it has been shown that the optical spectra of lead halide organic/inorganic perovskites can be easily tailored by varying the organic cation, which improves the optical efficiencies and tuning of the emission wavelength.¹⁹ Among them, self-assembled layered structures have recently shown enhanced non-linear optical properties in microcavities.²⁰ Interestingly, in these materials DFT calculations predict reversed ordering of band-edge states as compared to

tetrahedrally-bonded semiconductors.²¹ Consistently with important relativistic effects expected for lead, such calculations have also evidenced the major role of spin-orbit coupling (SOC) that significantly reduces the band-gap by inducing a large splitting of the first degenerated conduction levels.²¹

Surprisingly, for the hybrid 3D materials recently proposed as efficient DSSC,^{5,7,8,14-16} the effect of SOC has been largely overlooked, especially from the theoretical point of view. Optical absorption²² and reflectivity²³ measurements brought clear experimental evidence of sizeable SOC splittings in such materials more than a decade ago. Even so effects of SOC have been stressed in a recent computational work,¹⁵ to the best of our knowledge they have not yet been accounted for in calculated band structures reported in the literature.

This paper aims to investigate the role of SOC on the electronic band structure of two 3D hybrids recently investigated for PV-devices, namely MAPbX₃ compounds where X=Br,I and MA stands for methylammonium (CH₃NH₃). Moreover, as the design of efficient DSSC requires a good understanding of VB alignments, we suggest a protocol to derive the band alignment between the MAPbX₃ absorbers and TiO₂. It involves calculations on a slab of a related 2D hybrid, namely 2(C₄H₉NH₃⁺)(PbI₄²⁻).²⁴ Such analogs also allow further comparison and offer complementary routes for band gap engineering. Actually, by mixing the composition of halogen atoms in MAPb(I_{1-x}Br_x)₃ structures, it has recently been shown that the band gap can be controllably tuned to cover the entire visible spectrum.¹⁴

These mixed compounds exhibit an averaged disordered cubic phase (space group Pm3m) at room temperature.²⁵ The structural disorder is both associated to the rotation of ammonium cations and tilt of lead halide octahedra. At low temperature, MAPbBr₃ and MAPbI₃ present an

ordered orthorhombic structure of space-group $Pnma$, with a cell doubling when compared to the room temperature phase(Figure 1).^{15,26}

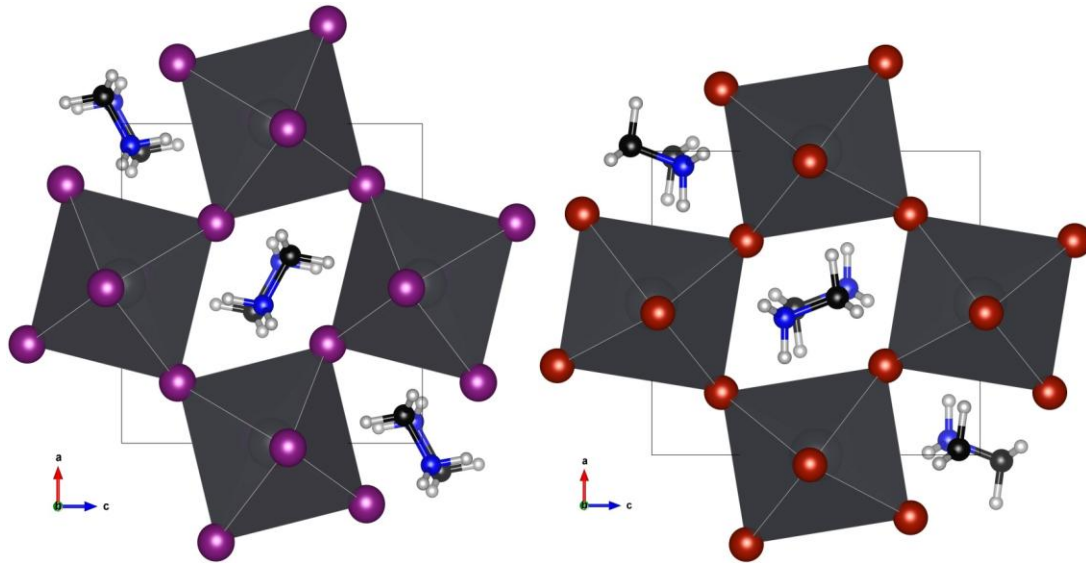
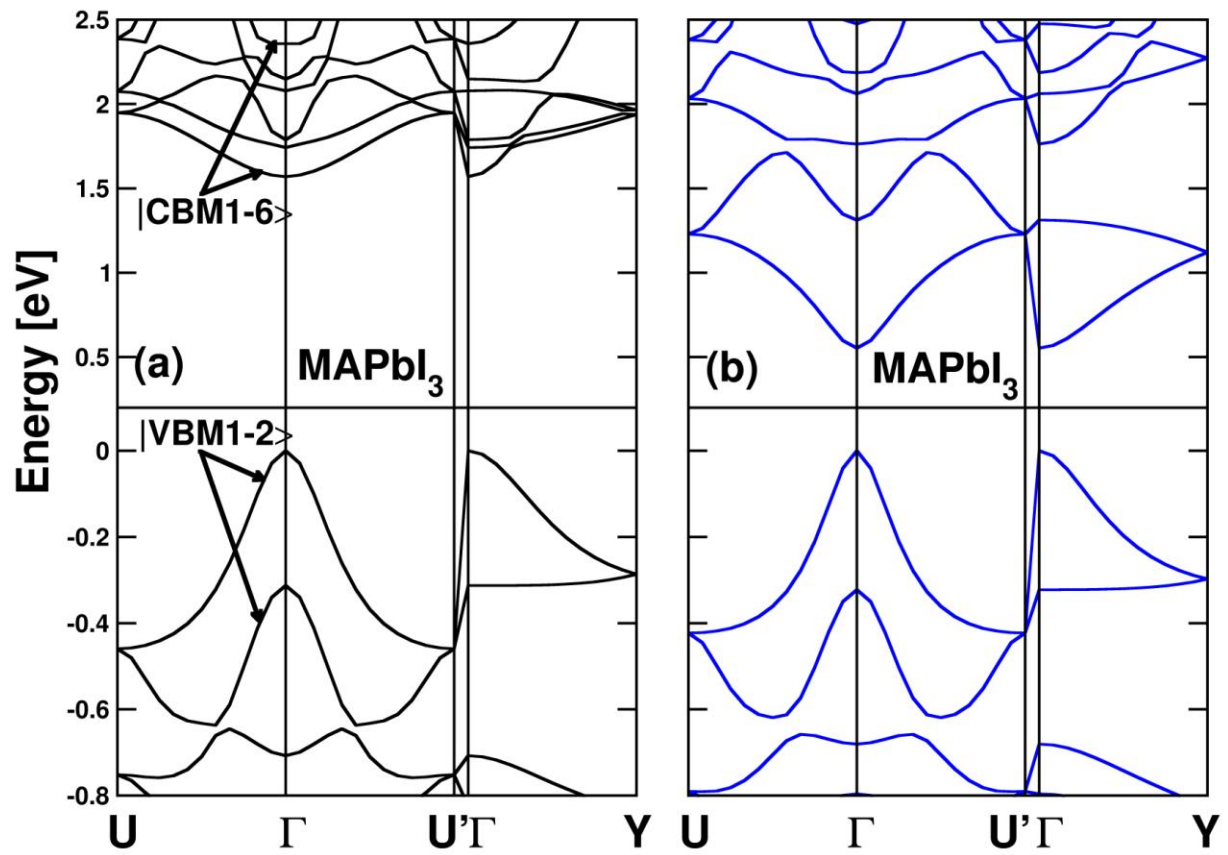


Figure 1. Overview of the crystal structures of MAPbI_3 (left) and MAPbBr_3 (right) at low temperature. The structures are both orthorhombic (space group $Pnma$),^{15,26} with a cell doubling when compared to the room temperature cubic phase.

These ordered crystalline structures are used to perform the present theoretical study. Figure 2 shows the band structures of MAPbBr_3 and MAPbI_3 with and without the SOC interaction.



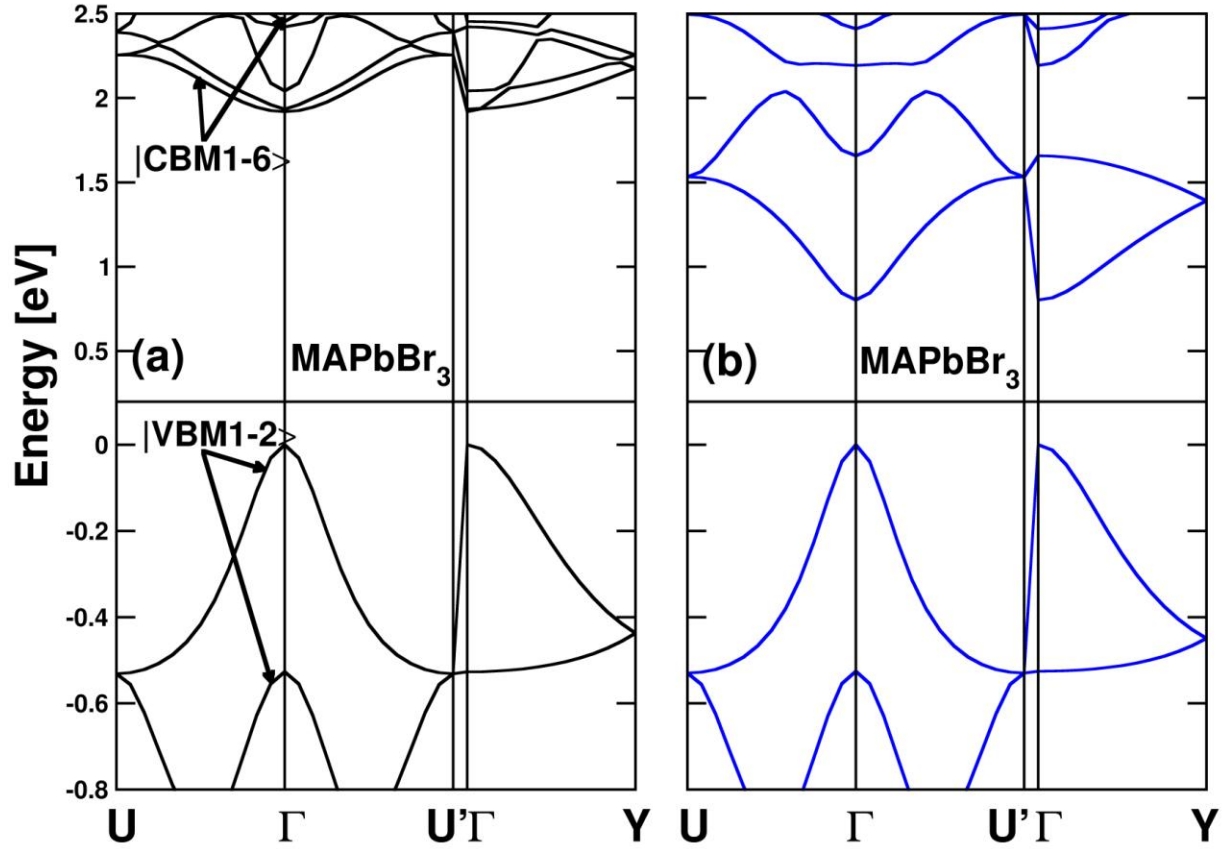


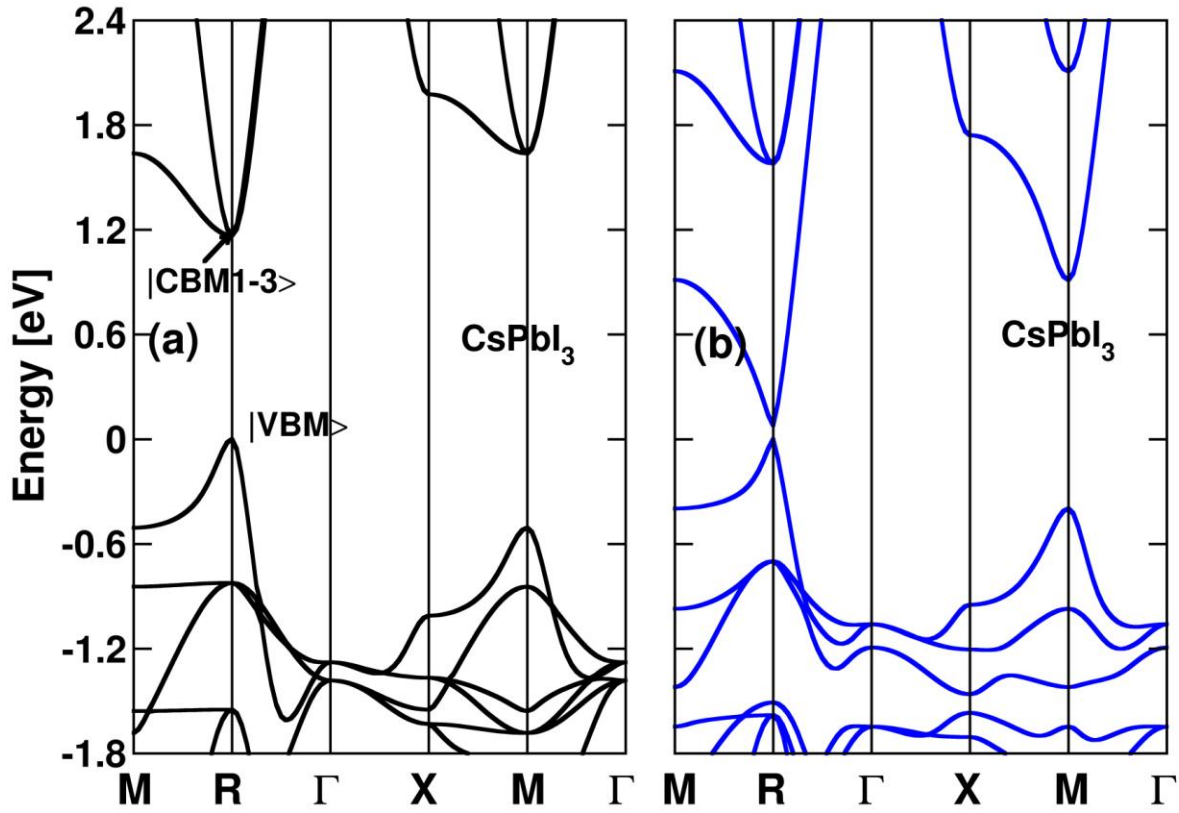
Figure 2. Electronic band structures of MAPbI₃ (top) and MAPbBr₃ (bottom), without (a) and with (b) the spin-orbit coupling interaction. The origin of the energy scale is taken at the top of the valence band (VBM).

Let us first analyze the results obtained without SOC. Consistently with earlier results on the room temperature cubic phase,²⁷ the ground state transitions are of direct type but at the Γ -point instead of the R point.¹⁵ Our study shows that they mainly involve eight active Bloch levels: two levels for the valence-band maximum (VBM1-2) and six levels for the conduction-band minimum (CBM1-6). This apparent complex sequence at Γ -point is associated to the low temperature symmetry breaking which leads both to unit cell doubling and strain.²⁶ In fact, a symmetry analysis indicates that the CBM1-6 states are related to the conduction-band minimum

(CBM) at the R point in the room temperature Pm3m cubic phase which corresponds to a triply-degenerate level associated to the vectorial representation of the simple group.²⁵ The same electronic band structure is obtained around the band gap for the related CsPbI₃ compound where the organic part of MAPbI₃ is replaced by a Cs atom in the low temperature Pnma phase (figure S1). We can further develop the analysis of the electronic states using the complete phase sequence of MAPbI₃ and CsPbI₃ structures (vide infra). Similar energy dispersions occur at low temperature along the Γ -U (1/2,0,1/2), Γ -Y and Γ -U' (1/2,0,-1/2) directions in figure 2, which is inherent to the small distortion of the perovskite lattice. The direct band-gap calculated at Γ -point is in agreement with the strong absorbance observed at room temperature.^{7,22} The six CBM1-6 states correspond to anti-bonding hybridizations of 6p-orbitals of lead and belong to the irreducible representations of the D_{2h} point group (factor group for the Pnma space group at Γ point). VBM1-2 consist in anti-bonding hybridizations of the 6s-orbitals of lead and 5p-orbitals of iodine and are associated to non-polar irreducible representations of the point group. Optical activity is related to the dipolar matrix elements between the first valence and conduction-band states as defined by: $M_{VBM,CBM1-3} = \left\langle \psi_{VBM} \left| -i\hbar \frac{\partial}{\partial x_i} \right| \psi_{CBM1-3} \right\rangle$ where x_i represents the crystal axis.²¹ These matrix elements take similar values for the CBM states in the MAPbX₃ family. A strong and almost isotropic optical activity is expected from symmetry and enhanced at room temperature by the disorder of the cubic phase. Similar results are obtained for MAPbI₃, although the strain-induced conduction-band splitting is larger. We point out that a strain effect was also reported in related MASnX₃ compounds.³²

Figure 2 reveals large changes of the electronic band structure when accounting for SOC. Indeed, the fundamental transitions of MAPbI₃ and MAPbBr₃ lower to 0.5eV and 0.8eV respectively.

While the VB are nearly unaffected, the sixfirst CB undergo a dramatic splitting. The band gap remains direct and located at the center of the Brillouin zone. These findings are consistent with the value reported for a related 2D organic–inorganic hybrid, $2(\text{pF-C}_6\text{H}_5\text{C}_2\text{H}_4\text{-NH}_3)\text{PbI}_4$, for which the correction is of about 1eV, leading to a band-gap reduction by a factor of two.²¹ This 2D perovskite crystalizes similarly to the $2(\text{AA})\text{PbX}_4$ family ($\text{AA} = \text{C}_n\text{H}_{2n+1}\text{NH}_3$)^{24,29,30} for which we have employed the same level of theory. For $n=4-12$ and $\text{X}=\text{I}$, the spin-orbit coupling induces a large band-gap correction of about 0.8eV, again mainly localized on the CB levels. Moreover, when applied to related inorganic structures such as CsPbX_3 , comparable corrections are obtained, as illustrated figure 3(top) for the inorganic cubic phase of CsPbI_3 (a similar result (figure S2) is obtained for the cubic phase of CsPbBr_3 .²⁵)



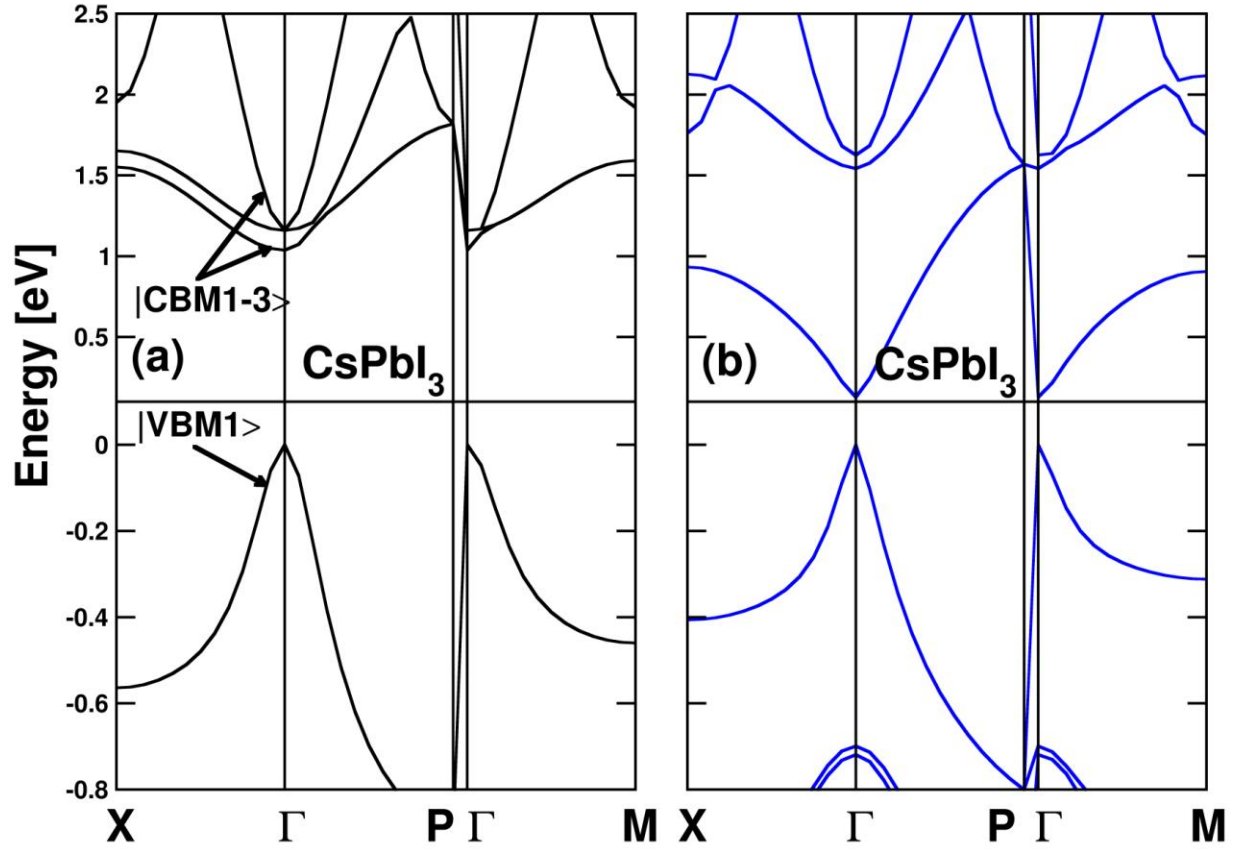


Figure 3. Electronic band structures of CsPbI_3 in the cubic phase (top) and tetragonal phase (bottom), without (a) and with (b) the spin-orbit coupling interaction. The origin of the energy scale is taken at the top of the valence band (VBM).

One can notice that the calculated band-gap at the GGA-PBE level is equal to 1.3eV in good agreement with previous simulations.³⁶ The calculated band-gaps at the LDA level are equal to 1.2eV for CsPbI_3 and 1.3eV for CsPbBr_3 , and the spin-orbit coupling induces a large band-gap correction of about 1.1eV in both cases (figure 3(top)). All these results demonstrate that the effect of SOC on band gaps is huge and cannot be reasonably disregarded. Even if comparison with available experimental data is not straightforward, our results are in qualitative good agreement with evidence of SOC effects in the optical absorption²² and reflectivity²³ spectra

reported for MAPbX₃. Furthermore, the optical transition occurs at the R point in the room temperature Pm3m cubic phase. For the Pm3msymmorphic space group, it is possible to directly analyze the irreducible representations at R point using the Oh point group.³¹ The triply-degenerate (CBM1-3) (figure 3-a (top)) states are associated to the vectorial representation of the simple group commonly described^{21,32} by the $|X\rangle$, $|Y\rangle$, $|Z\rangle$ symbols. In the corresponding double group including spinors, it is splitted by SOC into twofold degenerate states and fourfold degenerate states (figure 3-b (top)). This situation is usually encountered in the valence band of cubic conventional semiconductors.^{21,31} The conduction band minimum of CsPbX₃ and MAPbX₃ at room temperature are associated to the twofold degenerate spin-orbit split-off (SO) states

$$|1/2, 1/2\rangle = \frac{1}{\sqrt{3}}(|X + iY\rangle \uparrow) + \frac{1}{\sqrt{3}}|Z \downarrow\rangle \text{ and } |1/2, -1/2\rangle = \frac{1}{\sqrt{3}}(|X - iY\rangle \downarrow) + \frac{1}{\sqrt{3}}|Z \uparrow\rangle$$

(figure 3-b (top)). The SO states lead to a strong²¹ and isotropic³² optical transition with the even $|S\rangle$ -like VBM states. To understand the influence of the cubic-tetragonal (Pm3m-I4mcm) transition of MAPbI₃³³ on its optoelectronic properties, we have also performed DFT calculations on CsPbI₃ in the tetragonal phase of MAPbI₃ including the SOC. Without SOC, the triply degenerate CBM states and the VBM state are folded back from the R point at the Γ point cases (figure 3a, bottom). In addition and according to the D4h point group, the strain along the z axis induces a small splitting of the CBM and the band gap reduces to 1.0 eV. The CBM vectorial representation splits into a non-degenerate $|Z\rangle$ state at lower energy and twofold degenerate $|X\rangle$, $|Y\rangle$ states. The SOC effect is however much larger than the effect of strain, and leads to a very small band gap (figure 3b (bottom)). The state ordering including SOC at the Γ point of the I4mcm phase remains similar to the one of the Pm3m cubic phase, the CBM states being again related to the twofold degenerate SO states $|1/2, 1/2\rangle$ and $|1/2, -1/2\rangle$.

Based on the band structure of CsPbI_3 , we can also investigate the cubic-orthorhombic ($\text{Pm}3\text{m}$ - Pnma) transition. This transition is associated to a cell doubling and folding back from the R point to the Γ point. The triply degenerate CBM are doubled and splitted by the strain along the three directions. The six CBM states correspond to one dimensional representations of the simple $\text{D}_{2\text{h}}$ point group which yield two-fold degenerate representations of the corresponding double group. The strain effect is no more negligible when compared to the SOC effect, but the CBM state of lowest energy has an electronic density similar to the one of cubic SO state.

Now, one can wonder why the fundamental transitions calculated without SOC for the low temperature Pnma structures, 1.5 eV and 1.9 eV respectively for MAPbI_3 and MAPbBr_3 (figure 2) compare nicely with the values obtained experimentally, i.e. 1.5eV and 2.3eV respectively for MAPbI_3 and MAPbBr_3 .^{5,14,22,23} This agreement is fortuitous and stems from large error cancellations. Indeed, the band gap is known to be underestimated in the DFT ground-state computations. This can be corrected by including many-body effects by means of GW self-energy correction for the band gap³⁴ or using the Bethe Salpeter equation resolution for the exciton.³⁵ Unfortunately, such calculations are beyond available computational resources for large systems. In order to gauge the importance of the GW corrections, we have considered the cubic phase of CsPbI_3 . A one-shot GW self-energy correction on the LDA level amounts to a 0.6 eV increase of the band gap. This value, although not self-consistent, shows that GW corrections are large and in the opposite direction to SOC effects. Unfortunately, a full treatment including both SOC and many-body effects is far beyond available computational resources.

Efficient electrical power generation relies on the quality of the absorber and the band-gap energy. These conditions appear to be fulfilled and understood from the theoretical point of view. This efficiency also relies on the ability of the PV device to drive the carriers toward the

electrodes. A correct band alignment between the sensitizer and the electrode materials is thus a key parameter to predict performances of PV devices. In the case of DSSC, with a TiO_2 electrode, hybrid MAPbX_3 perovskites appear to greatly improve the electron transport.⁸ To evaluate the valence-band alignment between the anatase structure of TiO_2 ⁸ and hybrid perovskites, a slab calculation³⁷ was performed for the $2(\text{AA})\text{PbI}_4$ with $n=4$. This allows estimating the offsets between the vacuum level and its bulk potential (figure 4).

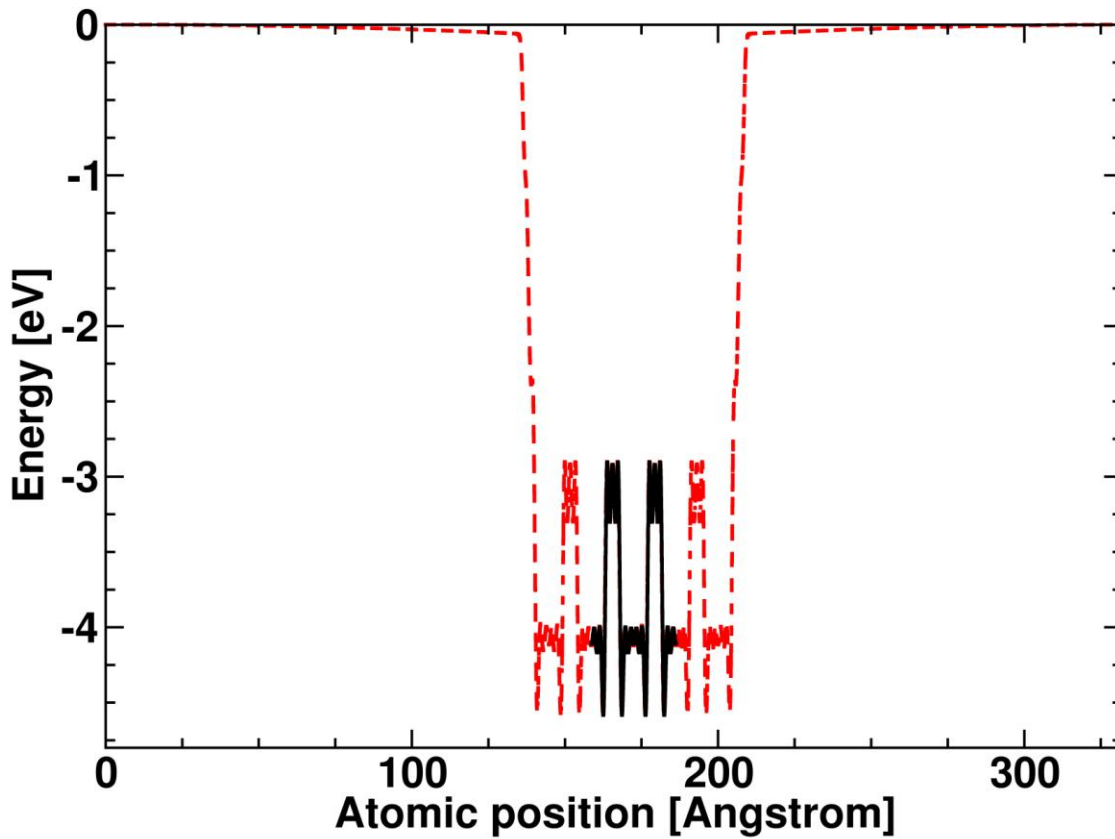


Figure 4. Potential profile in an alkyl ammonium (AA) 2D hybrid perovskite crystal (dark line) and in a slab (red dotted line) with the same crystallographic structure²⁴ surrounded by vacuum. An upward energy shift equal to 0.93 eV has been applied to the crystal profile in order to match the slab profile. When the same shift is applied to the computed VBM, an absolute VBM of -5.6 eV is found.

It leads to an absolute valence-band energy of -5.6 eV. Moreover, one can use the position of the 5d levels of lead as a common electronic marker both for 3D and 2D hybrid perovskites. The relative position of the 5d-orbitals with respect to their VBM amount respectively to -16.4 and -16.2 eV. This leads to an absolute valence-band energy of -5.4 eV for both MAPbX₃ crystals that nicely agrees with the absolute valence-band energy levels deduced from the experimental work functions: -5.44 and -5.38 eV for X=I and X=Br, respectively.⁵ The complete band alignment diagram is given figure 5, based on the absolute valence-band energy (-7.3 eV) commonly used for TiO₂.⁸

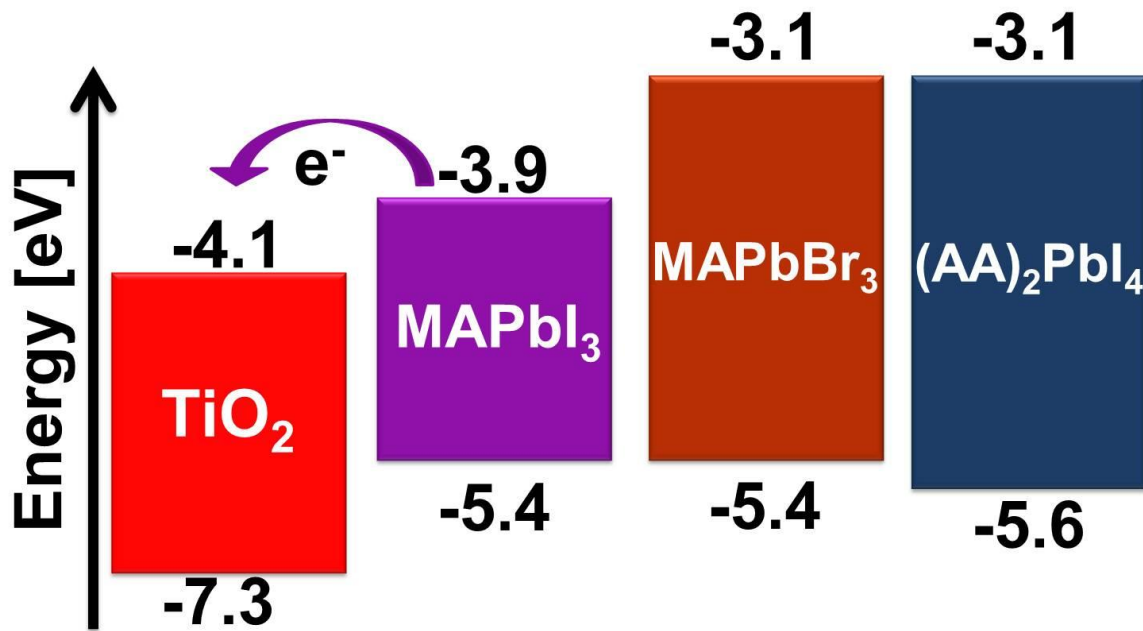


Figure 5. Energy level diagram derived from the position of Pb-5d orbitals, computed VBM (figure 4) and experimental band gaps of MAPbI₃ (1.5 eV), MAPbBr₃ (2.3 eV)^{5,14} and an alkyl ammonium (AA) 2D hybrid perovskite (2.5 eV).²⁴ Commonly accepted values for TiO₂ electron affinity of -4.1 eV and absolute valence band energy of -7.3 eV are used.

It clearly demonstrates that the conduction-band offsets are favorable for the electron injection from absorber to electrode. In addition, this diagram suggests that combining 2D and 3D hybrid perovskites may provide an alternative way for the design of colorful solar cells that cover the entire visible spectrum.

In summary, based on DFT calculations, the electronic properties of 3D lead halide organic/inorganic perovskites used as absorbers in DSSC^{5,7,8} have been thoroughly investigated. Their band-gap is dominated by a giant SOC effect acting mainly on the conduction band, as was already demonstrated for related 2D hybrids.²¹ At room temperature, their remarkable optical properties can be related to direct and isotropic optical transitions between a triply degenerated conduction-band and a single valence-band in a simple group representation. Valence band offsets⁵ confirm that the gathering of MAPbX₃ hybrids and TiO₂ is a relevant choice for driving the electrons toward the electrode. Our calculations on alkyl ammonium based 2D hybrids also suggest a complementary route to the *chemical tuning*¹⁴ recently proposed for the design of colorful solar cells with enhanced light conversion efficiency.

The present theoretical study was performed using the DFT implementation available in the ABINIT package,³⁸ with the LDA or the GGA-PBE gradient correction for exchange-correlation³⁹ and relativistic, norm-conserving, separable, dual-space Gaussian-type pseudopotentials of Goedecker, Teter, and Hutter for all atoms⁴⁰ or Fritz-Haber-Institute's pseudopotentials.⁴¹ The SIESTA code was used for the simulation of slabs at the DFT-GGA level.⁴² We have verified that the band structures near the band-gap do not depend on the inclusion of 5d-orbitals for Pb. The electronic wave-functions are expanded onto a plane-wave basis set with an energy cut-off of 950 eV. 4x4x4 and 4x4x1 Monkhorst-Pack grids are used for

reciprocal space integration in 3D and 2D structures respectively. Calculations were performed with and without SOC.

Corresponding Author

*Email: claudine.katan@univ-rennes1.fr Tel: +33 (0)2 23 23 56 82

Notes

The authors declare no competing financial interests.

This work was performed using HPC resources from GENCI-CINES/IDRIS grant 2013-c2012096724. The work is supported by Agence Nationale pour la Recherche (PEROCAI project ANR-10-04).

- (1) Feltrin, A.; Freundlich, A., Material considerations for terawatt level deployment of photovoltaics. *Renewable Energy* **2008**, *33* (2), 180-185.
- (2) Oregan, B.; Grätzel, M., A Low-cost, high-efficiency solar-cell based on dye-sensitized colloidal TiO₂ films. *Nature* **1991**, *353* (6346), 737-740.
- (3) Grätzel, M., Solar energy conversion by dye-sensitized photovoltaic cells. *Inorg. Chem.* **2005**, *44* (20), 6841-6851.
- (4) Almosni, S.; Robert, C.; Thanh, T. N.; Cornet, C.; Letoublon, A.; Quinci, T.; Levallois, C.; Perrin, M.; Kuyyalil, J.; Pedesseau, L.; Balocchi, A.; Barate, P.; Even, J.; Jancu, J. M.; Bertru, N.; Marie, X.; Durand, O.; Le Corre, A., Evaluation of InGaPN and GaAsPN

materials lattice-matched to Si for multi-junction solar cells. *J. Appl. Phys.* **2013**, *113* (12), 123509-123509-6.

- (5) Kojima, A.; Teshima, K.; Shirai, Y.; Miyasaka, T., Organometal Halide Perovskites as Visible-Light Sensitizers for Photovoltaic Cells. *J. Am. Chem. Soc.* **2009**, *131* (17), 6050-6051.
- (6) Im, J. H.; Lee, C. R.; Lee, J. W.; Park, S. W.; Park, N. G., 6.5% efficient perovskite quantum-dot-sensitized solar cell. *Nanoscale* **2011**, *3* (10), 4088-4093.
- (7) Lee, M. M.; Teuscher, J.; Miyasaka, T.; Murakami, T. N.; Snaith, H. J., Efficient Hybrid Solar Cells Based on Meso-Superstructured Organometal Halide Perovskites. *Science* **2012**, *338* (6107), 643-647.
- (8) Etgar, L.; Gao, P.; Xue, Z. S.; Peng, Q.; Chandiran, A. K.; Liu, B.; Nazeeruddin, M. K.; Gratzel, M., Mesoscopic $\text{CH}_3\text{NH}_3\text{PbI}_3/\text{TiO}_2$ Heterojunction Solar Cells. *J. Am. Chem. Soc.* **2012**, *134* (42), 17396-17399.
- (9) Kim, H. S.; Lee, C. R.; Im, J. H.; Lee, K. B.; Moehl, T.; Marchioro, A.; Moon, S. J.; Humphry-Baker, R.; Yum, J. H.; Moser, J. E.; Grätzel, M.; Park, N. G., Lead Iodide Perovskite Sensitized All-Solid-State Submicron Thin Film Mesoscopic Solar Cell with Efficiency Exceeding 9%. *Sci. Rep.* **2012**, *2*, 591-591-7.
- (10) Heo, J. H.; Im, S. H.; Noh, J. H.; Mandal, T. N.; Lim, C. S.; Chang, J. A.; Lee, Y. H.; Kim, H. J.; Sarkar, A.; Nazeeruddin, M. K.; Grätzel, M.; Seok, S. I., Efficient inorganic-organic hybrid heterojunction solar cells containing perovskite compound and polymeric hole conductors. *Nat. Photonics* **2013**, *7* (6), 487-492.

- (11) Ball, J. M.; Lee, M. M.; Hey, A.; Snaith, H. J., Low-temperature processed meso-superstructured to thin-film perovskite solar cells. *Energy & Environmental Science* **2013**, 6 (6), 1739-1743.
- (12) Baikie, T.; Fang, Y. N.; Kadro, J. M.; Schreyer, M.; Wei, F. X.; Mhaisalkar, S. G.; Graetzel, M.; White, T. J., Synthesis and crystal chemistry of the hybrid perovskite (CH₃NH₃) PbI₃ for solid-state sensitised solar cell applications. *J. Mater. Chem. A* **2013**, 1 (18), 5628-5641.
- (13) Qiu, J. H.; Qiu, Y. C.; Yan, K. Y.; Zhong, M.; Mu, C.; Yan, H.; Yang, S. H., All-solid-state hybrid solar cells based on a new organometal halide perovskite sensitizer and one-dimensional TiO₂ nanowire arrays. *Nanoscale* **2013**, 5 (8), 3245-3248.
- (14) Noh, J. H.; Im, S. H.; Heo, J. H.; Mandal, T. N.; Seok, S. I., Chemical Management for Colorful, Efficient, and Stable Inorganic-Organic Hybrid Nanostructured Solar Cells. *Nano Lett.* **2013**, 13 (4), 1764-1769.
- (15) Mosconi, E.; Amat, A. ; K. Nazeeruddin, Md. ; Grätzel, M. ; De Angelis, F., First Principles Modeling of Mixed Halide Organometal Perovskites for Photovoltaic Applications. *J. Phys Chem. C* **2013** (DOI: 10.1021/jp4048659)
- (16) Park, N.G., Organometal Perovskite Light Absorbers Toward a 20% Efficiency Low-Cost Solid-State Mesoscopic Solar Cell. *J. Phys Chem. Lett.* **2013**, 4, 2423-2429.
- (17) Burschka, J.; Pellet, N.; Moon, S.J.; Humphry-Baker, R.; Gao, P.; Nazeeruddin, M.K.; Grätzel, M.; Sequential deposition as a route to high-performance perovskite-sensitized solar cells *Nature* **2013** 499, 316–319.

- (18) Itzhaik, Y.; Hodes, G.; Cohen, H., Band Alignment and Internal Field Mapping in Solar Cells. *J. Phys. Chem. Lett.* **2011**, 2 (22), 2872-2876.
- (19) Mitzi, D. B.; Wang, S.; Feild, C. A.; Chess, C. A.; Guloy, A. M., Conducting layered organic-inorganic halides containing (110)-oriented perovskite sheets. *Science* **1995**, 267 (5203), 1473-1476.
- (20) Wei, Y.; Lauret, J. S.; Galmiche, L.; Audebert, P.; Deleporte, E., Strong exciton-photon coupling in microcavities containing new fluorophenethylamine based perovskite compounds. *Opt. Express* **2012**, 20 (9), 10399-10405.
- (21) Even, J.; Pedesseau, L.; Dupertuis, M. A.; Jancu, J. M.; Katan, C., Electronic model for self-assembled hybrid organic/perovskite semiconductors: Reverse band edge electronic states ordering and spin-orbit coupling. *Phys. Rev. B* **2012**, 86 (20), 205301-205301-4.
- (22) Tanaka, K.; Takahashi, T.; Ban, T.; Kondo, T.; Uchida, K.; Miura, N., Comparative study on the excitons in lead-halide-based perovskite-type crystals $\text{CH}_3\text{NH}_3\text{PbBr}_3/\text{CH}_3\text{NH}_3\text{PbI}_3$. *Solid State Comm.* **2003**, 127 (9-10), 619-623.
- (23) Hirasawa, M.; Ishihara, T.; Goto, T., Exciton features in 0-dimensional, 2-dimensional, and 3-dimensional networks of PbI_6 4-octahedra. *J. Phys. Soc. Jap.* **1994**, 63 (10), 3870-3879.
- (24) Billing, D. G.; Lemmerer, A., Synthesis, characterization and phase transitions in the inorganic-organic layered perovskite-type hybrids $(\text{C}_n\text{H}_{2n+1}\text{NH}_3)_2\text{PbI}_4$, $n=4, 5$ and 6 . *Acta Cryst. B* **2007**, 63, 735-747.

- (25) Poglitsch, A.; Weber, D., Dynamic disorder in methylammonium trihalogenoplumbates(II) observed by millimeter-wave spectroscopy. *J. Chem. Phys.* **1987**, *87* (11), 6373-6378.
- (26) Swainson, I. P.; Hammond, R. P.; Soulliere, C.; Knop, O.; Massa, W., Phase transitions in the perovskite methylammonium lead bromide, $\text{CH}_3\text{ND}_3\text{PbBr}_3$. *J. Solid State Chem.* **2003**, *176* (1), 97-104.
- (27) Umebayashi, T.; Asai, K.; Kondo, T.; Nakao, A., Electronic structures of lead iodide based low-dimensional crystals. *Physical Review B* **2003**, *67* (15), 155405-155405-6.
- (28) Chiarella, F.; Zappettini, A.; Licci, F.; Borriello, I.; Cantele, G.; Ninno, D.; Cassinese, A.; Vaglio, R., Combined experimental and theoretical investigation of optical, structural, and electronic properties of $\text{CH}_3\text{NH}_3\text{SnX}_3$ thin films ($\text{X}=\text{Cl}, \text{Br}$). *Phys. Rev. B* **2008**, *77* (4), 045129-045129-6.
- (29) Billing, D. G.; Lemmerer, A., Synthesis, characterization and phase transitions of the inorganic-organic layered perovskite-type hybrids $(\text{C}_n\text{H}_{2n+1}\text{NH}_3)_2\text{PbI}_4$ ($n=12, 14, 16$ and 18). *New J. Chem.* **2008**, *32* (10), 1736-1746.
- (30) Lemmerer, A.; Billing, D. G., Synthesis, characterization and phase transitions of the inorganic-organic layered perovskite-type hybrids $(\text{C}_n\text{H}_{2n+1}\text{NH}_3)_2\text{PbI}_4$, $n=7, 8, 9$ and 10 . *Dalton Trans.* **2012**, *41* (4), 1146-1157.
- (31) Bir, G.L.; Pikus, G.E., Symmetry and strain-induced effects in semiconductors, New York Toronto : Wiley **1974**
- (32) Chuang, S., Physics of Optoelectronic Devices, J. W. Goodman ed., New York: Wiley, **1995**

- (33) Kawamura, Y.; Mashiyma, H.; Hasebe, K. Structural Study on Cubic-Tetragonal Transition of $\text{CH}_3\text{NH}_3\text{PbI}_3$. *J. Phys. Soc. Jpn.* **2002**, 71, 1694-1697.
- (34) Hedin, L., New method for calculating 1-particle greens function with application to electron-gas problem. *Phys. Rev.* **1965**, 139 (3A), A796-A823.
- (35) Salpeter, E. E.; Bethe, H. A., A relativistic equation for bound-state problems. *Phys. Rev.* **1951**, 84 (6), 1232-1242.
- (36) Murtaza, G.; Ahmad, I., First principle study of the structural and optoelectronic properties of cubic perovskites CsPbM_3 (M=Cl, Br, I). *Physica B* **2011**, 406 (17), 3222-3229.
- (37) Prodhomme, P. Y.; Fontaine-Vive, F.; Van der Geest, A.; Blaise, P.; Even, J., Ab initio calculation of effective work functions for a TiN/HfO₂/SiO₂/Si transistor stack. *Appl. Phys. Lett.* **2011**, 99 (2), 022101-022101-3.
- (38) Gonze, X.; Amadon, B.; Anglade, P. M.; Beuken, J. M.; Bottin, F.; Boulanger, P.; Bruneval, F.; Caliste, D.; Caracas, R.; Cote, M.; Deutsch, T.; Genovese, L.; Ghosez, P.; Giantomassi, M.; Goedecker, S.; Hamann, D. R.; Hermet, P.; Jollet, F.; Jomard, G.; Leroux, S.; Mancini, M.; Mazevet, S.; Oliveira, M. J. T.; Onida, G.; Pouillon, Y.; Rangel, T.; Rignanese, G. M.; Sangalli, D.; Shaltaf, R.; Torrent, M.; Verstraete, M. J.; Zerah, G.; Zwanziger, J. W., ABINIT: First-principles approach to material and nanosystem properties. *Comp. Phys. Comm.* **2009**, 180 (12), 2582-2615.
- (39) Perdew, J. P.; Burke, K.; Ernzerhof, M., Generalized gradient approximation made simple. *Phys. Rev. Lett.* **1996**, 77 (18), 3865-3868.
- (40) Hartwigsen, C.; Goedecker, S.; Hutter, J., Relativistic separable dual-space Gaussian pseudopotentials from H to Rn. *Phys. Rev. B* **1998**, 58 (7), 3641-3662.

- (41) Fuchs, M; Scheffler, M., Ab initio pseudopotentials for electronic structure calculations of poly-atomic systems using density-functional theory, *Comp. Phys. Comm.* **1999**, *119*(1), 67-98.
- (42) Soler, J. M.; Artacho, E.; Gale, J. D.; Garcia, A.; Junquera, J.; Ordejon, P.; Sanchez-Portal, D., The SIESTA method for ab initio order-N materials simulation. *J. Phys. Cond. Mat.* **2002**, *14* (11), 2745-2779.